DELPHI Collaboration

2002-079-CONF-613
24th July 2002

A Study of excited *b*-hadron states with the DELPHI Detector at LEP

Z. Albrecht, G. Barker, M. Feindt, U. Kerzel, M. Moch, L. Ramler
Institut für Experimentelle Kernphysik, Universität Karlsruhe
P. Kluit
NIKHEF, Amsterdam

Abstract

New analyses from DELPHI concerning the spectroscopy of excited B states from the LEP data set of the years 1992-98 are reported. Two different approaches and the use of modern techniques together with a complete re-processing of the data set, allow a revision of old DELPHI results published or presented at conferences. All results given here are preliminary. Within one approach the production rate of narrow $B^{**}_{u,d}$ states - assuming that they can be described by a single Gaussian - is measured to

$$\frac{\sigma(B^{**}_{u,d})_{narrow}}{\sigma_b} = 0.098 \pm 0.007 \pm 0.012$$

where data suggest the presence of broad states.
For B^{**}_s and $\Sigma^{(*)}_b$ upper limits on the production rates are obtained:

$$\sigma(B^{**}_s)/\sigma_b < 0.015, \quad \sigma(\Sigma^{(*)}_b)/\sigma_b < 0.015 \quad @\ 95\% CL$$

which supersede previous DELPHI results on these states.

Contributed Paper for ICHEP 2002 (Amsterdam)

1 Introduction and Motivation

This paper reports on a search for orbitally excited, i.e. $L = 1$, B-mesons and the excited b-baryon states $\Sigma_b^{(*)}$ in DELPHI $Z^0 \to b\bar{b}$ events taken in the years 1992 to 1998. Searches are made in the channels:

$$\begin{aligned} B_u^{+**} &\to B^{(*)0}\pi^+ \\ B_d^{0**} &\to B^{(*)+}\pi^- \\ B_s^{0**} &\to B^{(*)+}K^- \\ \Sigma_b^{(*)\pm} &\to \Lambda_b^0\pi^\pm \end{aligned}$$

and their charge conjugated states. Throughout this paper we will collectively refer to these states as b^{**}.

The motivation for a study of b-excited states is threefold:

(1) The analyses presented here represent the result of applying much improved and extended techniques of spectroscopy to a data set that has been completely re-processed, particularly with respect to the particle tracking, since an earlier DELPHI publication [1] based on data from 1991-1993.

(2) All measurements report a rather high value for the $B_{u,d}^{**}$ production rate, i.e. in the region of 25-30% (see Section 2 for an overview) . This conclusion needs verification, in particular because all analyses use the simulation to subtract the background. Studies using different generators have shown that significant differences in the description of the background can exist which could contribute a serious systematic effect in analyses where the background levels are high. For this reason, it is crucial to focus on analyses which either operate at working points where the background levels are low or employ methods where the sensitivity to simulation is reduced as much as possible.

(3) Preliminary signals for the B_s^{**} and $\Sigma_b^{(*)}$ states have been presented by DELPHI as conference submissions in the past [2] and it is important to clarify their status. The results presented in this paper should therefore be regarded as superseding any previous DELPHI publication or conference submission on this subject.

After an overview of current results on b^{**} spectroscopy and a brief description of the DELPHI detector, this paper describes two complementary approaches to the study of b-excited states: The first, which we term the 'high purity approach', inclusively tags the b^{**} states by neural networks trained on variables correlated to the decay of an excited state at the primary event vertex by emission of an associated charged π- or K-primary track. The purity of the signal can thus be enhanced by making successively harder cuts on the neural network output. The background is taken from the simulation but its normalisation is left free in the fit. The second method, termed the 'high efficiency approach', takes the background from data itself by making a simultaneous fit to the data for the signal and background in samples enriched and depleted in b^{**} states. This procedure reduces significantly the dependence of the MC description on the background situated below the b^{**} peak. The paper concludes with a summary and conclusions section.

2 Overview

Central to theoretical predictions in the spectroscopy of b-hadron states is the utilisation of an approximate heavy flavour symmetry arising from the fact that the mass of the b-quark is large relative to the scale Λ_{QCD}. In the resulting theoretical framework of Heavy Quark Effective Theory (HQET) [3], the spin of the b-quark ($\vec{S}_b$) in a hadron is conserved in production and decay processes *independently* of the total angular momentum of the light quark spectator system ($\vec{J}_{light} = \vec{S}_{light} \oplus \vec{L}$). Excitation energy levels are thus doublets in *total spin* J of the hadron and the different states can be labelled in terms of the spin-parity of the hadron, J^P and the total spin of the light-quark system, J_{light}. The states within each doublet should be degenerate in mass by HQET and have the same strong interaction width, however the $1/m_b$ corrections turn out to be important in nature and act to break the degeneracy. A primary motivation for studying excited b-states is to test the predictions of non-perturbative models based on HQET and so make progress in understanding the true nature of the QCD potential. A further motivation comes from the observation [4] that a large production rate of excited states would be useful in tagging the b-quark flavour (i.e. b or $\bar{b}$) of a b-hadron at the time of its production. This already is providing a powerful tool for flavour tagging [5, 6] which is an essential part of B^0 oscillation and CP-violation studies.

Primary mesons can be produced in an orbitally excited ($L = 1$) state or in an $L = 0$ state. In the case of $L = 0$ and $J_{light} = 1/2$ there are two possible spin states: $J^P = 0^-$ corresponding to the pseudoscalar (P) weakly decaying ground states B^+, B^0 and B_s^0 and $J^P = 1^-$ which is the vector (V) state B^*. From simple $(2J+1)$ spin counting, one would expect the relative production rate of these states to be $V/(V+P) = 0.75$ [1] which turns out to be in good agreement with measurements of the B^* production rate [7, 8] using $B^* \to B\gamma$ decays.

For the orbitally excited states with $L = 1$, the quark model predicts *four* different (B^{**}) meson states. The dominant decay mode of $B^{**}_{u,d}$ is expected to be into $B^{(*)}\pi$ where the notation indicates that the B and B^* states are not discriminated. HQET groups these four states into two sets of degenerate doublets: the first doublet corresponding to $J_{light} = 1/2$ has one state with the assignment $J^P = 0^+$ and three degenerate states with $J^P = 1^+$. The second doublet has $J_{light} = 3/2$ where there are three degenerate states corresponding to $J^P = 1^+$ and five more corresponding to $J^P = 2^+$. The predicted properties of the B^{**} meson states are listed in Table 1 and their expected spectroscopy is shown graphically in Figure 1.

The members of the $J_{light} = 3/2$ doublet are expected to be very narrow compared to typical strong decay widths since only $L = 2$ (D-wave) transitions are allowed. This follows, for the case of the $J^P = 2^+$ state, from angular momentum and parity conservation and from a dynamical prediction for the case of the $J^P = 1^+$ state [3, 10].

Evidence for the existence of $B^{**}_{u,d}$ states first emerged in analyses at LEP in which a charged pion produced at the primary event vertex was combined with an inclusively reconstructed B-meson [1, 8, 11] resulting in an average $B^{**}_{u,d}$ mass of between 5700 and 5730 MeV. In a subsequent analysis, the ALEPH Collaboration performed an analysis combining a primary charged pion with a fully reconstructed B meson [6] and measured the mass of the B_2^* to be $5739^{+8}_{-11}(\text{stat})^{+6}_{-4}(\text{syst})$ MeV in a fit to the mass spectrum which

[1] Corrections to this due to the influence of excited B states are predicted to be small.

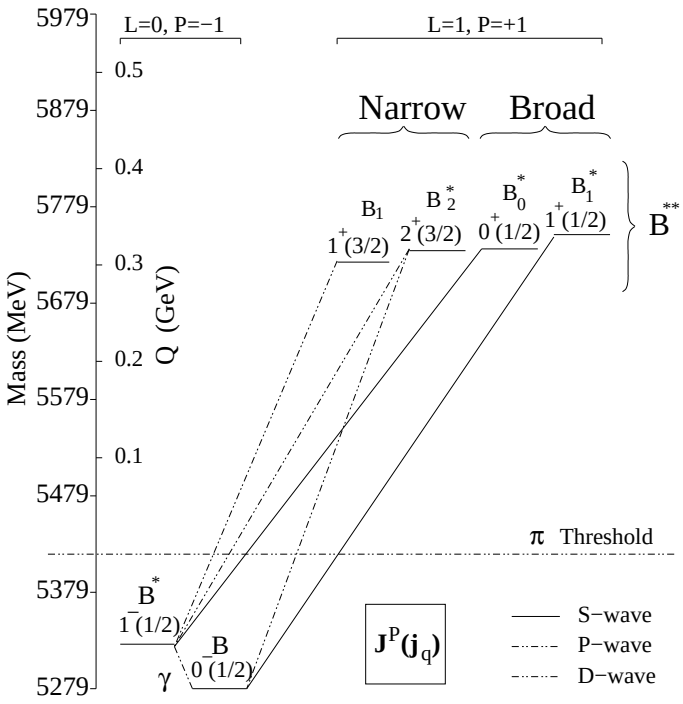

Figure 1: The spectroscopy of the ground state B-mesons and the oribitally excited B^{**} states (adapted from [9]).

J_{light}	J^P	B^{**} state	Decay Mode	Transition	Prod. Rate
1/2	0^+	B_0^*	$B\pi$	S-wave	1
1/2	1^+	B_1^*	$B^*\pi$	S-wave	3
3/2	1^+	B_1	$B^*\pi$	D-wave	3
3/2	2^+	B_2^*	$B^*\pi, B\pi$	D-wave	5

Table 1: The four $B_{u,d}^{**}$ states and their expected spin/parity assignments and decay properties. Also listed are the relative production rates of the states based on (2J+1) spin counting.

fixed the mass differences, widths and relative rates of all spin states according to the predictions of [12]. ALEPH also reported a $B_{u,d}^{**}$ production rate of $31 \pm 9(stat.)^{+6}_{-5}(syst.)\%$.

The L3 Collaboration have presented a measurement of the mass and width of the B_1^* and B_2^* states by a constrained fit to the mass spectrum obtained by a combination of a primary charged pion with an inclusively reconstructed B meson [13]. The constraints imposed reflect the current level of understanding regarding the widths and masses of the B^{**} states:

- In the D-meson sector, the two narrow states with $J_{light} = 3/2$ have been clearly identified experimentally [14] and the spin-parity and decay characteristics have been shown to be in accord with the HQET predictions. By extrapolating from these measurements, one can expect that the widths of the $J_{light} = 3/2$ states are approximately equal and in the range $20 - 25$ MeV. For the case of the $J_{light} = 1/2$ states, there are no corresponding measurements in the D system and so the prediction is based only on the theoretical expectation that the widths are approximately equal

albeit rather broader than for the $J_{light} = 3/2$ states.

- There is a consensus amoung existing HQET-based predictions (see e.g. Refs. [12], [15] to [20]) that the mass difference between the two $J_{light} = 1/2$ and the two $J_{light} = 3/2$ states, should be approximately equal and in the range $5 - 20$ MeV.
- There is however a disagreement between current models regarding the absolute size of the masses with some models [16, 17] predicting the average mass of $J_{light} = 3/2$ states should be larger than that of the $J_{light} = 1/2$ states and others [19, 20], predicting the opposite.

More recently the CDF Collaboration have presented the first results on $B^{**}_{u,d}$ production from a hadron collider [9] by combining a charged primary pion to a partially reconstructed B using semileptonic decays to charm. They measure the (model dependent) mass of the lowest B^{**} state to be $M_{B_1} = 5.71 \pm 0.02$ GeV/c^2 and the production rate of $B^{**}_{u,d}$ to be $0.28 \pm 0.06(stat.) \pm 0.03(syst.)$.

For the case of the B^{**}_s, if the meson mass is above the $B^{(*)}K$ threshold, this will be the dominant decay mode since the $B_s\pi$ channel is forbidden by isospin invariance. The predictions from HQET presented in Table 1 for $B^{**}_{u,d}$ now carry over with the replacement of the primary decay pion by a kaon. Experimentally, evidence for the B^{**}_s is less compelling than for the $B^{**}_{u,d}$ and, to date, OPAL [11] in the only collaboration reporting a significant signal. They see an excess over background of 149 ± 31 B^+K^- pairs (with invariant masses in the range 5.80-6.00 GeV), which translates into,

$$\frac{BR(Z^0 \to \bar{b} \to B^{**0}_s \to B^{(*)+}K^-)}{BR(Z^0 \to \bar{b} \to B^+)} = 0.026 \pm 0.008$$

(Note that the same analysis also quotes: $BR(Z^0 \to \bar{b} \to B^{0**} \to B^{(*)+}\pi^-)/BR(Z^0 \to \bar{b} \to B^+) = 0.18 \pm 0.04$)

No detailed numbers are known for the case of the primary hadron being a baryon, but flavour and spin counting rules indicate that a large fraction of primary b-baryons will be excited states e.g. Σ_b, Σ^*_b which will decay by either the electromagnetic or strong interaction into the lightest b-baryon state, the Λ_b. In addition to the Λ_b probably the only other weakly decaying b-baryons are the Ξ^-_b, Ξ^0_b and the Ω_b. Experimentally, there are currently no confirmed signals reported for the $\Sigma^{(*)}_b$ although there is evidence for Ξ_b production [21].

3 The DELPHI detector

A complete overview of the DELPHI detector [22] and its performance [23] have been described in detail elsewhere. What follows is a short description of the elements most relevant for this analysis.

Charged particle tracking was performed by the Vertex Detector (VD), the Inner Detector, the Time Projection Chamber (TPC) and the Outer Detector. A highly uniform magnetic field of 1.23 T parallel to the e^+e^- beam direction, was provided by the superconducting solenoid throughout the tracking volume. The momenta of charged particles (tracks) were reconstructed with a precision of $\sigma_p/p < 2.0 \times 10^{-3} \cdot p$ (p in GeV/c) in the polar angle region $25^\circ < \theta < 155^\circ$. The VD consisted of three layers of silicon micro-strip

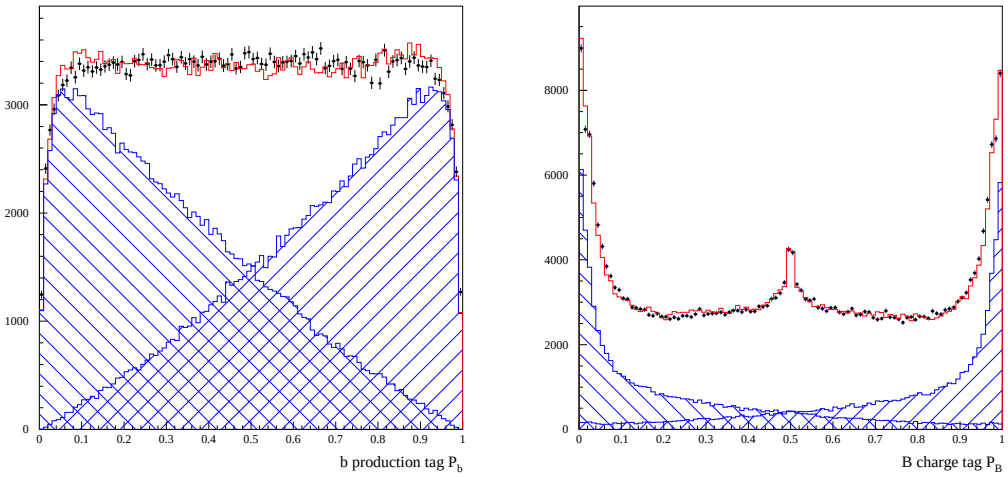

Figure 2: Distribution for the production tag P_b (left). The dots correspond to the 1992 to 1995 data, the solid line to the simulation. The hatched areas correspond to the b (left) and $\bar{\mathrm{b}}$ (right) contributions. The udsc quarks contribution is 9% and has not been shown explicitly on the plot. Distribution for the B vertex charge tag P_B (right). The dots correspond to the 1992-1995 data, the solid lines to the simulation. The hatched areas correspond to the B^+ (left) and B^- (right) contributions. The contributions from neutral B hadrons and the udsc quarks contribution are not shown explicitly on the plot.

devices with an intrinsic resolution of about 8 μm in the $R-\phi$ plane transverse to the beam line. In addition, the inner and outer-most layers were instrumented with double-sided devices providing coordinates of similar precision in the $R-z$ plane along the direction of the beams. For tracks with hits in all three $R\phi$ VD layers the impact parameter resolution was $\sigma^2_{R\phi} = ([61/(P\sin^{3/2}\theta)]^2 + 20^2)$ μm^2 and for tracks with hits in both Rz layers and with polar angle $\theta \approx 90^\circ$, $\sigma^2_{Rz} = ([67/(P\sin^{5/2}\theta)]^2 + 33^2)$ μm^2. Calorimeters detected photons and neutral hadrons by the total absorption of their energy. The High-density Projection Chamber (HPC) provided electromagnetic calorimetry coverage in the polar angle region $46^\circ < \theta < 134^\circ$ giving a relative precision on the measured energy E of $\sigma_E/E = 0.32/\sqrt{E} \oplus 0.043$ (E in GeV). In addition, each HPC module worked essentially as a small TPC charting the spatial development of showers and so providing an angular resolution exceeding that of the detector granularity alone. For high energy photons the angular precisions were ± 1.7 mrad in the azimuthal angle ϕ and ± 1.0 mrad in the polar angle θ.

The Hadron Calorimeter was installed in the return yoke of the DELPHI solenoid and provided a relative precision on the measured energy of $\sigma_E/E = 1.12/\sqrt{E} \oplus 0.21$ (E in GeV).

Powerful particle identification was made possible by the combination of dE/dx information from the TPC (and to a lesser extent from the VD) with information from the Ring Imaging CHerenkov counters (RICH) in both the forward and barrel regions. The RICH devices utilised both liquid and gas radiators in order to optimise coverage across a wide momentum range: liquid was used for the momentum range from 0.7 GeV/c to 8 GeV/c and the gas radiator for the range 2.5 GeV/c to 25 GeV/c.

4 Analyses

Two different analysis approaches have been used to search for excited B states. We will call them *High Purity Approach (HPA)* and *High Efficiency Approach (HEA)* throughout the paper.

4.1 Enrichment Techniques

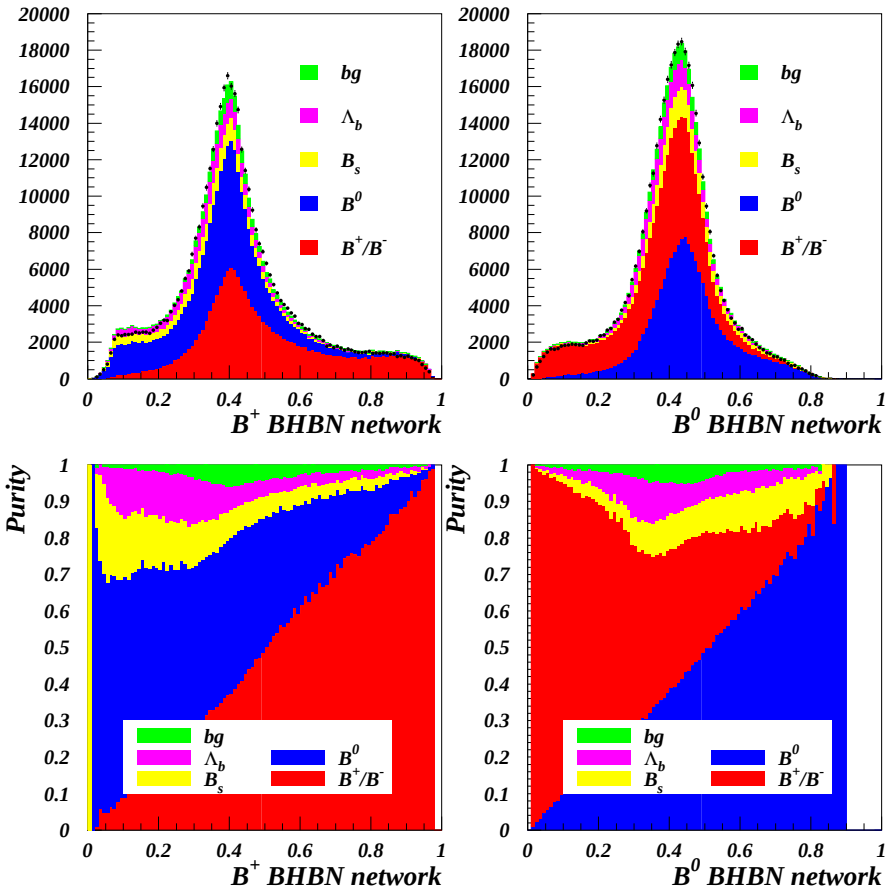

Figure 3: The upper plots show the output of the B^+ and B^0 output nodes of the neural network dedicated to distinguish between the different weakly decaying b-hadrons in the 1994 data. Overlaid is the b-hadron composition as seen in the Monte Carlo and the lower plots trace the change in purity per bin. The background, labelled 'bg' consists of light and charm quark events.

Common to both analyses was the reconstruction of the weakly decaying b hadron by using inclusive techniques. Detailed descriptions of these techniques can be found in [24] (HPA) and [25] (HEA). Cuts were applied to select pions (respectively kaons) originating from the primary vertex and to suppress background from fragmentation. To get enriched or depleted samples of b^{**}, correlations between the charge of the decay pions (kaons) and the b-flavour were used. When the decay particle was a pion, particle identification was

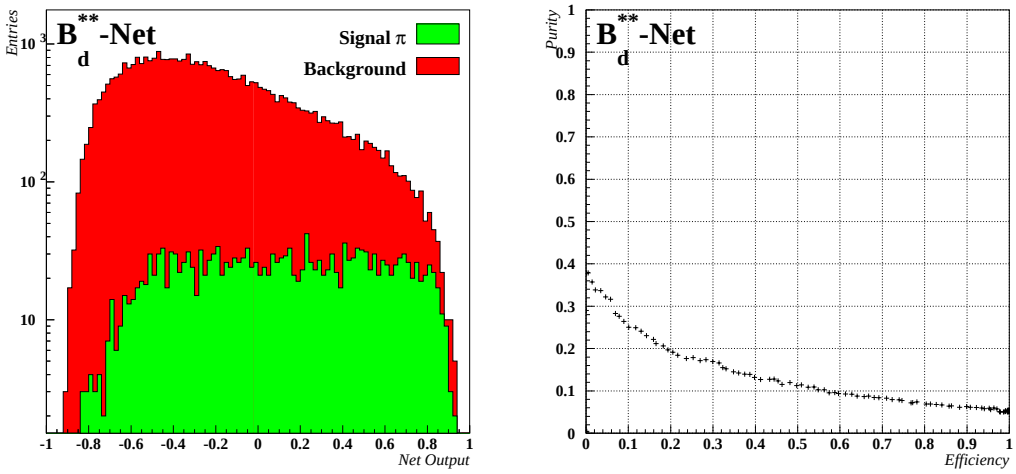

Figure 4: The left-hand plot shows the output of the B_d^{**} network. Signal means here the B_d^{**} decay pion. The right-hand plot shows its tagging efficiency against purity performance

used to suppress kaons and protons, for B_s^{**} it was used to enrich kaons [26, 27].

High Efficiency Approach

Relatively soft cuts were designed to produce similar background shapes in the enriched/depleted samples. The variables used for the flavour and charge tagging are shown in figure 2. In this way the background shapes could be extracted from the enriched/depleted samples of the data itself and fitted simultaneously, thus reducing the dependence on Monte Carlo models. This analysis was performed on data of the years 1992-95.

High Purity Approach

Dedicated neural networks were built for identification of the weakly decaying hadron (see figure 3), for B-momentum reconstruction, assignment of a track to primary or secondary vertex, charge correlation and for enrichment of the corresponding decay track (pion or kaon) of the different types of b^{**} hadrons. To prevent that the network could learn the signal Q-value all the neural networks for b^{**} were trained on a Monte Carlo sample with a flatly distributed signal in the Q-value. As example the output and the performance of the B_d^{**} net on a statistically independent Monte Carlo sample is shown in figure 4. Data of the years 1994-98 were used for this analysis.

4.2 Results for $B_{u,d}^{**}$

4.2.1 High Efficiency Approach

Selection of $B_{u,d}^{**}$ events

The $\overline{B_d^{**}}$ particle is selected using its decay into a B^- and a π^+. The corresponding signature will be the presence of a b quark correlated with a π^+ and a charged B^- meson in the same event hemisphere. The $\overline{B_u^{**}}$ particle is selected in its decays into a $\bar{B}_d^0$ and a

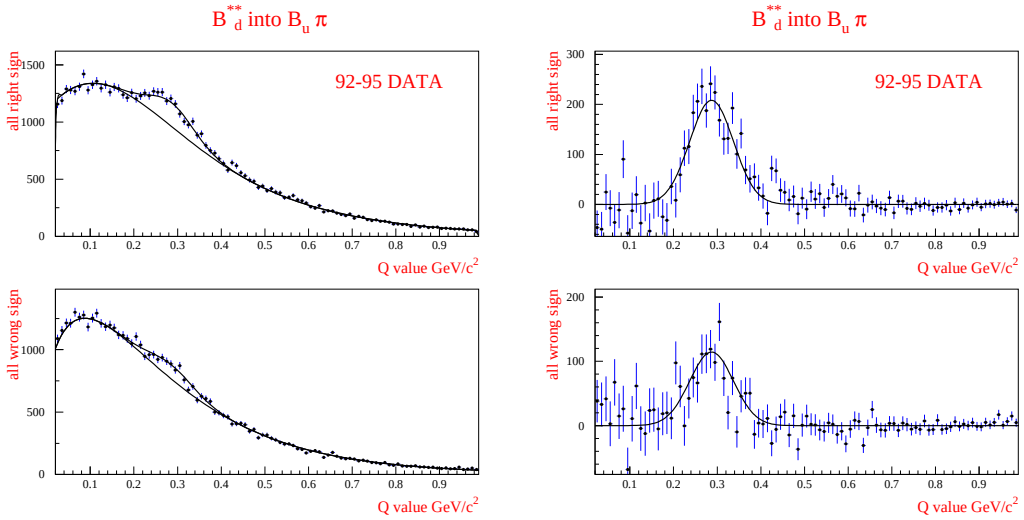

Figure 5: The Q distributions for the $\overline{B_d^{**}}$ signal enriched (top) and background enriched (bottom) samples. The result of the fit is superimposed. On the right, the Q distributions for the signal enriched (top) and background enriched (bottom) samples after subtraction of the fit result for the background. The result of the Gaussian signal fit is superimposed.

π^-. In this case one expects a b quark correlated with a π^- and a neutral B_d meson to be present in the same event hemisphere. Signals of the $\overline{B_d^{**}}$ and $\overline{B_u^{**}}$ particles can therefore be separated using the correlation between a b production tag and the charge of the pion. In the analysis a signal enriched and a background enriched sample have been selected. For this purpose cuts were applied to the B vertex charge.

The following cuts were applied to select $\overline{B_d^{**}}$ candidates:

- Signal enriched sample: $q_\pi(P_b - 0.5) < 0$ and $q_\pi(P_B - 0.5) > 0.2$
- Background enriched sample : $q_\pi(P_b - 0.5) < 0$ and $q_\pi(P_B - 0.5) < 0.2$

where P_b denotes the b production tag probability, P_B the B charge probability and q_π the pion charge. The distribution of the b production tag probability P_b is shown in Fig. 2 on the left where the separate contributions from b and $\overline{b}$ are given. The distribution of the B charge probability P_B is shown in Fig. 2 on the right.

For the selection of $\overline{B_u^{**}}$ candidates the following cuts were applied:

- Signal enriched sample: $q_\pi(P_b - 0.5) > 0$ and $q_\pi(P_B - 0.5) > -0.4$
- Background enriched sample: $q_\pi(P_b - 0.5) > 0$ and $q_\pi(P_B - 0.5) < 0.4$

Description of the Q distribution

The cuts defined above were designed to produce rather similar shapes for the non $B_{u,d}^{**}$ background in the signal enriched and in the background enriched samples. The Q distribution for the signal enriched sample is described as:

$$S(Q) = S_{B^{**}}(Q) + BKG(Q)\ (a_0 + a_1 Q), \tag{1}$$

where $S_{B^{**}}(Q)$ is the $B_{u,d}^{**}$ signal shape: for a narrow resonance a Gaussian distribution is used and a Breit-Wigner shape with a mass dependent width is taken for a broad resonance. The background enriched sample, B, is expressed as:

$$B(Q) = \epsilon\ S_{B^{**}}(Q) + BKG(Q) \tag{2}$$

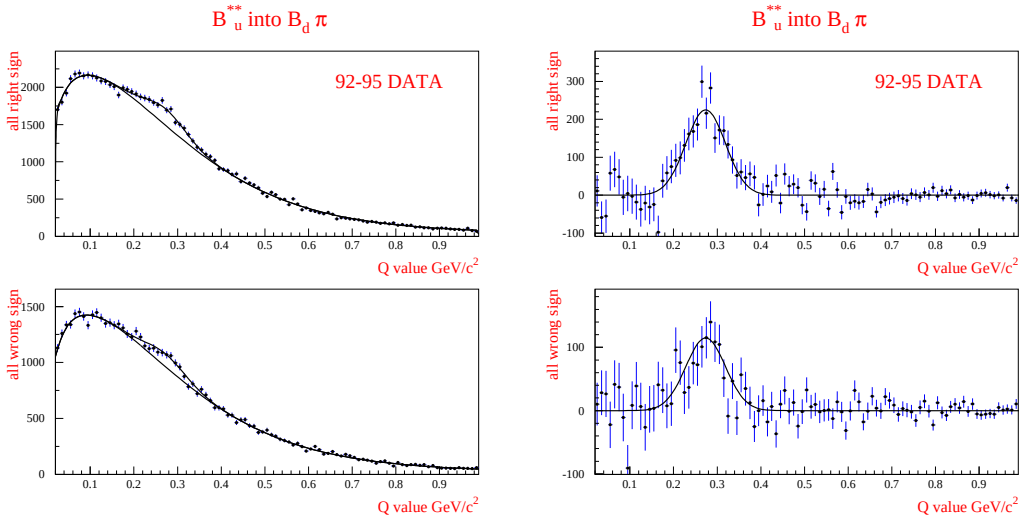

Figure 6: The Q distributions for the signal (top) and background (bottom) enriched samples (left). The result of the fit is superimposed. On the right, the Q distributions for the $\overline{B_u^{**}}$ signal (top) and background (bottom) enriched samples after subtraction of the fit result for the background. The result of the Gaussian signal fit is superimposed.

$\epsilon(< 1)$ corresponds to the depletion of the $B_{u,d}^{**}$signal in this sample relative to the enriched sample.

In the above equations, the background Q distribution BKG, has been parametrized as:

$$BKG(Q) = ERF(Q)\, b_0 e^{-b_1 Q - b_2 Q^2 - b_3 Q^3 - b_4 Q^{\kappa}}, \tag{3}$$

where ERF is a threshold function:

$$ERF(Q) = (e^{-\alpha Q} - e^{\alpha Q})/(e^{-\alpha Q} + e^{\alpha Q}) + \beta \tag{4}$$

It was verified extensively on the simulation that the signal and background enriched samples can be described by these functions. Of particular importance is the fact that the background in the signal enriched sample S can be described with only two additional parameters a_0 and a_1, where a_1 is small.

Fit to the $B_{u,d}^{**}$ spectra

The χ^2 fit was performed using the signal and background enriched sample in the Q value range from 0 to 1 GeV/c^2. Extensive tests were performed using the simulation of narrow B_d^{**} states corresponding to the B_2^* (5.771 GeV/c^2) and the B_1 (5.759 GeV/c^2) with a production rate of 3:2. The total observed signal corresponding to the two particles could be described by a single Gaussian distribution having a Q value of 290 MeV/c^2 and a width of 60 MeV/c^2. For a single resonance, that decays exclusively into either Bπ or B$^*\pi$, one would expect a width of 52 MeV/c^2.

For the $\overline{B_d^{**}}$ spectrum, the value of ϵ was 0.549, κ was 0.5, as determined using simulated events. The data were fitted leaving free the amplitude, the Q value and width of the Gaussian signal. Further, the parameters a_0, a_1 and b_0 to b_4 were left free. The parameters of the threshold function were fixed at $\alpha = 200$ and $\beta = 1$. A constraint was applied on the parameter a_1 of -0.033 ± 0.037. The $\chi^2/NDOF$ of the fit to the

$\overline{B_d^{**}}$ spectrum was 199/200-11 with the following results for the parameters:

$$\begin{aligned} \text{Q}&= (287 \pm 3)\ \text{MeV/c}^2 \\ \sigma &= (50 \pm 4)\ \text{MeV/c}^2 \\ \text{N}&= 2614 \pm 216, \end{aligned}$$

where N corresponds to the total number of events in the Gaussian signal. The quoted errors are statistical only. The results for the $\overline{B_d^{**}}$ spectrum are shown in Fig. 5.

For the $\overline{B_u^{**}}$ spectrum, the value of ϵ was 0.510, κ was 0.25, as determined using simulated events. The same fit was performed to the $\overline{B_u^{**}}$ spectrum. The parameters of the threshold function were fixed at $\alpha = 30$ and $\beta = 3$. A constraint was applied on the parameter a_1 of 0.115 ± 0.033. The $\chi^2/NDOF$ of the fit to the $\overline{B_u^{**}}$ spectrum was 198/200-11 with the following results for the parameters:

$$\begin{aligned} \text{Q}&= (274 \pm 4)\ \text{MeV/c}^2 \\ \sigma &= (46 \pm 4)\ \text{MeV/c}^2 \\ \text{N}&= 2560 \pm 245, \end{aligned}$$

where N corresponds to the total number of events in the Gaussian signal. The quoted errors are statistical only. The results for the $\overline{B_u^{**}}$ spectrum are shown in Figures 6.

Measurement of the $B_{u,d}^{**}$ production rate

From the observed number of events in the Gaussian signal peak, one can extract the production rate of $\overline{B_d^{**}}$ and $\overline{B_u^{**}}$ particles in a b quark jet. The results are:

$$\begin{aligned} \sigma_{\bar{B_d^{**}}}/\sigma_b &= 0.054 \pm 0.005(stat) \pm 0.006(sys). \\ \sigma_{\bar{B_u^{**}}}/\sigma_b &= 0.044 \pm 0.004(stat) \pm 0.006(sys). \end{aligned}$$

The total rate becomes:

$$\sigma_{\bar{B_{u,d}^{**}}}/\sigma_b = 0.098 \pm 0.007(stat) \pm 0.012(sys).$$

The systematic error is obtained by applying a tighter $B_{u,d}^{**}$ selection, leaving approximately half of the fitted events. The evaluated branching ratio was stable within 10%. The systematic errors for the $\overline{B_d^{**}}$ and $\overline{B_u^{**}}$ production rates were assumed to be fully correlated. There is no systematic error coming from background shapes used from the simulation, because the backgrounds were fitted on the data.

The shape and central value of the signal Q distribution

The Gaussian standard deviation of the $\overline{B_d^{**}}$ and $\overline{B_u^{**}}$ fitted signals is $47 \pm 3(sys) \pm 5(sys)$ MeV/c^2 and the average observed central Q value is 280 MeV/c^2. The systematic error was evaluated by applying a tighter $B_{u,d}^{**}$ selection. For a single narrow resonance one would expect a Gaussian width of 50 MeV/c^2. This means that the data prefer a single resonance. If the observed resonance consists of the B_2^* and B_1 particles both produced equally likely, the mass splitting between the two particles should be small, and the B_2^* decay into $B^*\pi$ should dominate.

The systematic error on the Q value has three components. Firstly, there is an average shift of the observed Q value of 18 MeV/c^2 estimated with an error of 3 MeV/c^2 using the

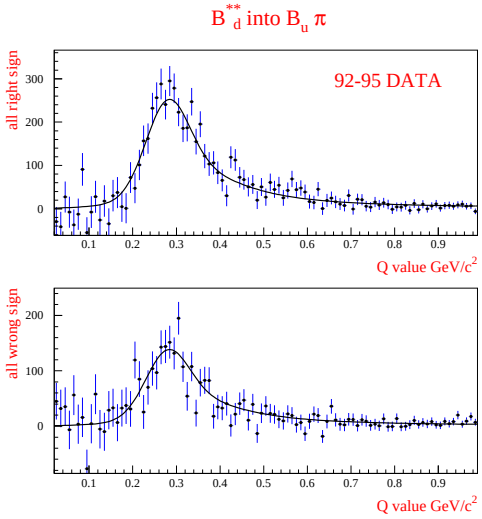

Figure 7: The Q distributions for the $\overline{B_d^{**}}$ signal enriched (top) and background enriched (bottom) samples after subtraction of the fit result for the background of the case of state counting. The result of the Gaussian signal fit plus a broad Breit-Wigner is superimposed.

simulation. The shift is due to a shift of the estimated B momentum in $B_{u,d}^{**}$ decays. Secondly, the Q values of the $\overline{B_u^{**}}$ and $\overline{B_d^{**}}$ mesons after reconstruction agree with each other within 4 MeV/c^2. Furthermore, the systematic uncertainty on the Q value determination mainly coming from the momentum uncertainty is estimated to 3%.

The Q value of the observed signal corresponds to:

$$\mathrm{Q} = (298 \pm 4 \pm 12)(sys)\ \mathrm{MeV/c^2}.$$

Search for Broad States

Adding broad components to the fit could improve the fits for both cases. This was done by fitting two additional parameters for a mass dependent Breit-Wigner distribution (the most probable value and the width) whereas the normalisation was fixed by setting the relative contribution of broad:narrow to 1:1 (state counting) or 1:2 (spin counting). The number of events in the Gaussian and the width were fixed to the values obtained previously. The χ^2 improvement was 22 adding 4 degrees of freedom, similar for both fits. The result after subtraction of the fitted background for the case of state counting for B_d^{**} is shown in figure 7.

4.2.2 High Purity Approach

Selection of $B_{u,d}^{**}$ Events

In contrast to the High Efficiency Approach, dedicated neural networks were trained for identifying the $B_{u,d}^{**}$ decay pion (see section 4.1) in order to perform an analysis with a signal-to-background ratio of approximately 1:1. By imposing a cut on the Charge Correlation (CC) which came from a dedicated neural network a 'right-sign' (r.s.) and 'wrong-sign' (w.s.) sample was defined as follows:

$$CC < -0.3, \quad B_u^{**+} \to B^0\pi^+, \ `right-sign'$$

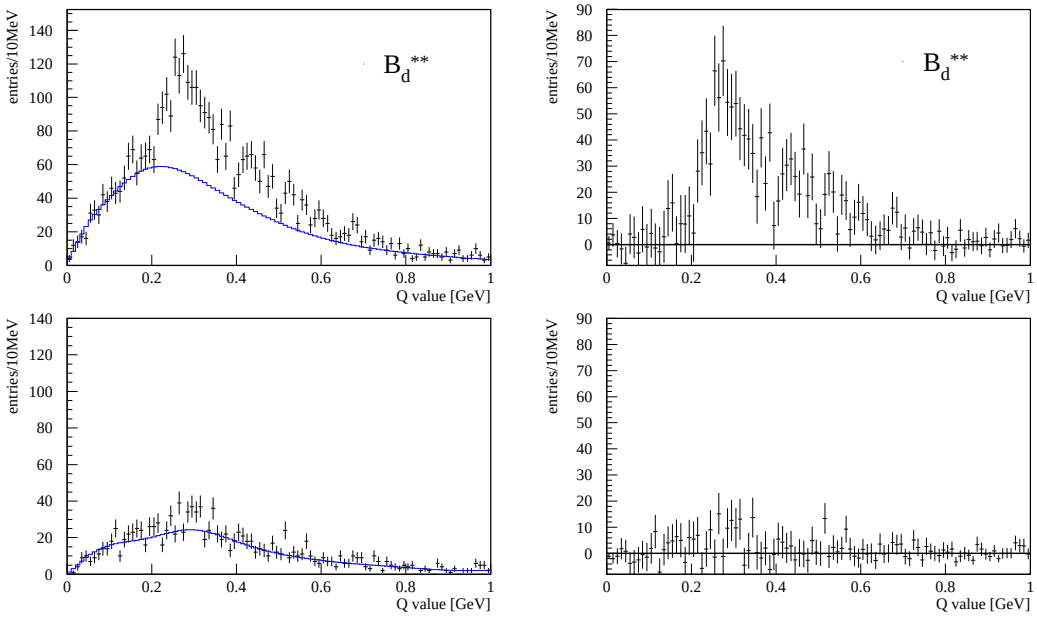

Figure 8: The Q-value distribution of the high purity B_d^{**} analysis. On the left the data distributions together with the fitted background, on the right the corresponding subtracted distributions. Plots of the right-sign (upper plot) and wrong-sign (lower plot) combination for the B^{0**} hypothesis.

$$
\begin{aligned}
CC > 0.3, \quad & B_u^{**+} \to B^0\pi^-, \quad `wrong-sign' \\
CC > 0.0, \quad & B_d^{**0} \to B^+\pi^-, \quad `right-sign' \\
CC < 0.0, \quad & B_d^{**0} \to B^+\pi^+, \quad `wrong-sign'
\end{aligned}
$$

This selection was applied to data and Monte Carlo events respectively. The correspomding spectra are shown in figures 8 and 9.

Fit to the $B_{u,d}^{**}$ Spectra

A fit to the B_d^{**} and B_u^{**} spectrum separately was performed assuming that the observed signal could be described by a single Gaussian with no contribution from broad $B_{u,d}^{**}$ or other excited states. The background taken from Monte Carlo was allowed to vary in the fit as a linear function of the Q-value:

$$\text{fitted bg} = \text{bg} \cdot (a + b \cdot Q),$$

a and b were free parameters in the fit. Although the background did not differ too much from the original Monte Carlo background, including a and b into the fit resulted in significantly better fit probabilities. The $\chi^2/NDOF$ of the fit to the B_d^{**} spectrum was 319/(200-5) with the following results:

$$Q = (290 \pm 4)\ \text{MeV/c}^2$$

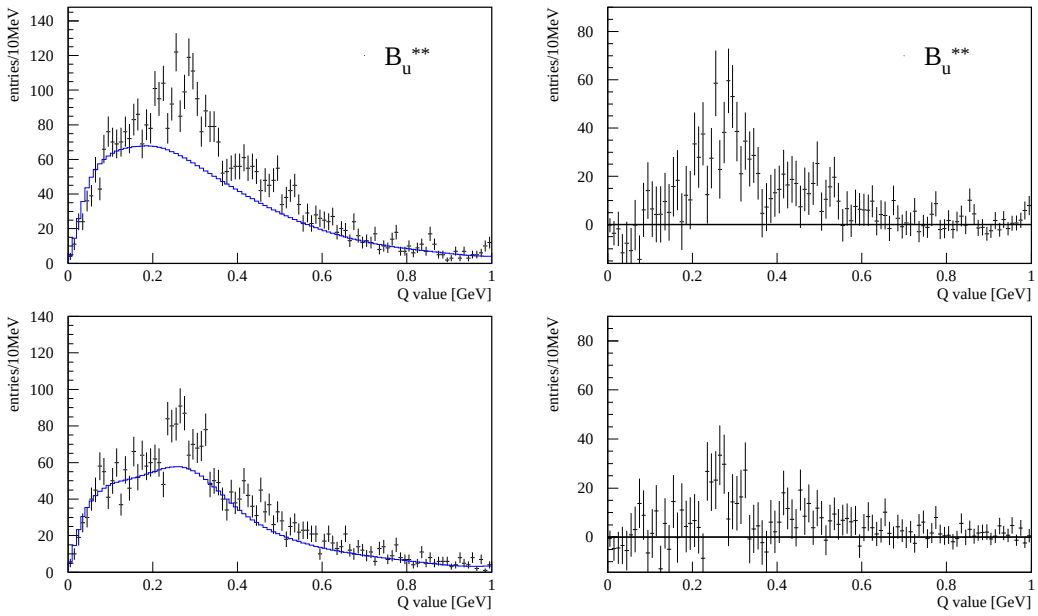

Figure 9: The Q-value distribution of the high purity B_u^{**} analysis. On the left the data distributions together with the fitted background, on the right the corresponding subtracted distributions. Plots of the right-sign (upper plot) and wrong-sign (lower plot) combination for the B^{+**} hypothesis.

$$\sigma = (51 \pm 5)\ \mathrm{MeV/c^2}$$
$$N = (665 \pm 60),$$

where N corresponds to the number of events in the Gaussian signal. The quoted errors are statistical only. The wrong sign sample is very well described by the fitted background. In the right sign sample a significant excess of events at the right side of the narrow signal is visible. Further investigations are necessary.

The B_d^0-$\bar{B}_d^0$ classification is much more complicated. This explains why the background for the B_u^{**} sample is obviously not yet perfectly described. The $\chi^2/NDOF$ of the fit to the B_u^{**} spectrum was 294/(200-5) with the following results:

$$Q = (278 \pm 5)\ \mathrm{MeV/c^2}$$
$$\sigma = (47 \pm 6)\ \mathrm{MeV/c^2}$$
$$N = (459 \pm 57),$$

where N corresponds to the number of events in the Gaussian signal. The quoted errors are statistical only. These results are in good agreement with those of the High Efficiency Approach but cannot give a good description of the signal. So additional contributions are needed, preferably at higher masses. Moreover, an excess in data can be seen in both cases around a Q-value of 450 $\mathrm{MeV/c^2}$. Taking this into account the fit quality is significantly improved. Further investigations are under way.

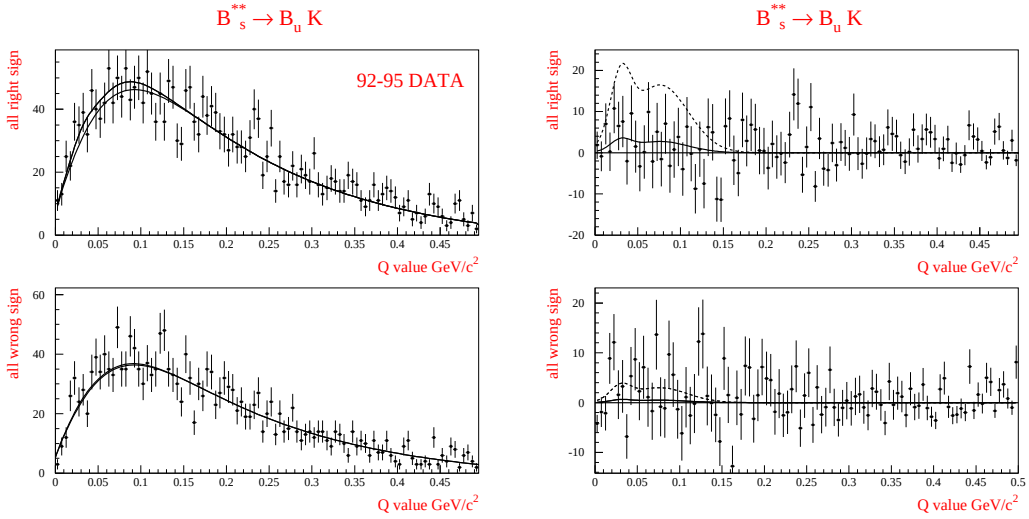

Figure 10: On the left the Q distributions for the $\overline{B_s^{**}}$ signal enhanced (top) and background enhanced (bottom) enriched samples. The result of the fit is superimposed. On the right the Q distributions for the B_s^{**} signal enhanced (top) and background enhanced (bottom) samples after subtraction of the fit result for the background. The result of the double Gaussian signal fit is superimposed. The dashed line corresponds to the expected signal for a $\overline{B_s^{**}}$ production rate of 3%.

4.3 Results for B_s^{**} and $\Sigma_b^{(*)}$

4.3.1 High Efficiency Approach

A search for $\overline{\mathrm{B_s^{**}}}$ particles

A similar approach is followed to search for the $\overline{B_s^{**}}$ in its decay into $\overline{\mathrm{B_u}}\mathrm{K}^+$. A signal enhanced and a background enhanced sample were selected applying the following cuts.

- identified charged kaons (standard or tight) were selected
- Signal enhanced sample: $q_\pi(P_b - 0.5) < 0$
- Background enhanced sample: $q_\pi(P_b - 0.5) > 0$

The cosine of the angle between the kaon and the B direction in the B rest frame, $\cos\psi$, had to be larger than -0.6. To select charged B particles it was required that $|P_B - 0.5| > 0.2$.

The Q spectrum was fitted using the same functions as described in section 4.2.1. The parameter κ was fixed to 0.5, ϵ to 0.18 and a_1 to 0 as obtained from simulation. The parameter β in the threshold function was fixed to 0.23 and α to 6.

The results for a fit with a signal consisting of two Gaussians, one centred at 30 MeV/c^2 and a width of 12 MeV/c^2 and one centred at 76 MeV/c^2 with a width of 33 MeV/c^2 are shown in Fig. 10 left . The values of the parameters of the Gaussians correspond to the values used in the simulation, which were based on the predictions of [12]. The χ^2/NDOF of the fit was 214/200-7. In total 71 signal events were fitted in the data with an error of 71 events. The difference between the observed events and the result of the fit is shown in Fig. 10 right. The dashed line corresponds to the signal one would expect for a total

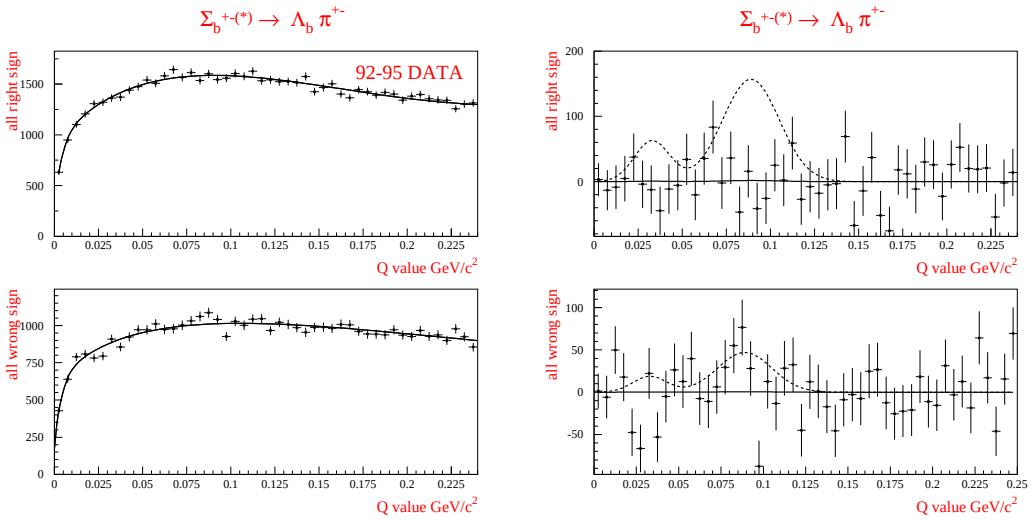

Figure 11: On the left the Q distributions for the signal enhanced (top) and background enhanced (bottom) $\Sigma_b^{(*)}$ samples. The result of the fit is superimposed. On the right the Q-value distributions for the $\Sigma_b^{(*)}$ signal enhanced (top) and background enhance (bottom) samples after subtraction of the fit result for the background. The dashed line corresponds to the expected signal for a $\Sigma_b^{(*)}$ production rate of 3%.

B_s^{**} $/\sigma_b$ production rate of 3%.

No narrow signal is observed in the Q value range up to 150 MeV/c^2, where the expected resolution is better than 30 MeV/c^2. The upper limit on the production rate for a narrow B_s^{**} resonance is:

$$\sigma_{\overline{B_s^{**}}}/\sigma_b < 0.015 \ \ at\ 95\%\ \mathrm{CL}$$

A search for $\Sigma_b^{(*)}$ particles

A similar approach is followed to search for the $\Sigma_b^{(*)}$ particles in their decay into $\Lambda_b \pi^{\pm}$. A signal enhanced and a background enhanced sample were selected applying the following cuts.

• Signal enhanced sample: $q_\pi(P_b - 0.5) < 0$ and $q_\pi(P_B - 0.5) < 0.2$ or $q_\pi(P_b - 0.5) > 0$ and $q_\pi(P_B - 0.5) > -0.3$

• Background enhanced sample: $q_\pi(P_b - 0.5) < 0$ and $q_\pi(P_B - 0.5) > 0.2$ or $q_\pi(P_b - 0.5) > 0$ and $q_\pi(P_B - 0.5) < -0.3$

The Q spectrum is fitted using the same functions as described in section 4.2.1. The parameter b_3 was fixed to 0, κ to 0.5 and ϵ to 0.30, as obtained from simulation. Two additional terms were added to the term $a_0 + a_1 Q$: $a_2 Q^2$ and $a_3 Q^3$ as it was observed that the ratio between the two background distributions had a more complicated Q dependence than a linear variation. The parameter β in the threshold function was fixed to 1 and α was left free to vary.

The results for a fit with a signal consisting of two Gaussians, one centred at 33 MeV/c^2 with a width of 10 MeV/c^2 and the other centred at 89 MeV/c^2 with a width of 16 MeV/c^2, are shown in Fig. 11 left. The parameters of the two Gaussians correspond to the preliminary signals observed in [2]. The χ^2/NDOF of the fit is 94/100-11. In total 22 signal events were fitted in the data with an error of 351 events. The difference between

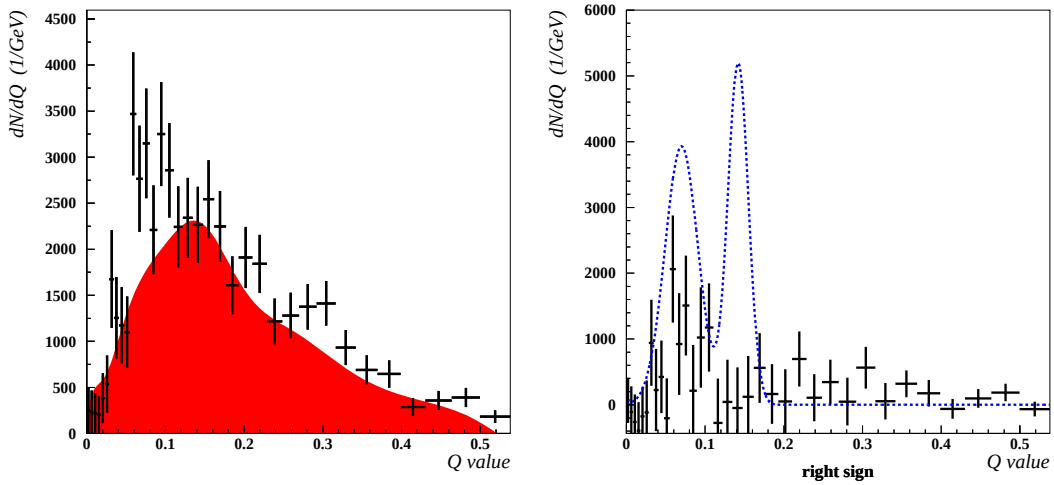

Figure 12: The left-hand plot shows a B_s^{**} enhanced Q-value distribution and the right-hand plot the background subtracted off, together with a comparison with the old DELPHI result giving a total production rate of 3.7%. The upper limit given in the text corresponds to the region at a Q-value of 70 MeV.

the observed events and the result of the fit is shown in Fig. 11 right. The dashed line corresponds to the signal one would expect for a total $\Sigma_b^{(*)}/\sigma_b$ production rate of 3%.

No narrow signal was observed in the Q value range up to 150 MeV/c^2 where the expected resolution is better than 30 MeV/c^2. The upper limit on the production rate for a narrow $\Sigma_b^{(*)}$ resonance is:

$$\sigma_{\Sigma_b^{(*)}}/\sigma_b < 0.015 \ \ at\ 95\%\ \mathrm{CL}$$

4.3.2 High Purity Approach

Selection of B_s^{**} Events

The method used to search for B_s^{**} states follows closely the neural network approach presented above for the $B_{u,d}^{**}$. The crucial difference in this case is that the primary charged track is a kaon instead of a pion.

To enhance B_s^{**} events a cut on the output of the dedicated B_s^{**} neural network was applied to give a signal to background ratio of approximately 50% at the signal Q-value region. The B_s^{**} network input variables also include the MACRIB kaon identification net output which boosts the performance of the B_s^{**} enrichment considerably. This allows a signal-to-background ratio comparable with the $B_{u,d}^{**}$ case although the expected production rate is an order of magnitude smaller.

To further enhance the signal purity, a 'right-sign' (r.s.) and a 'wrong-sign' (w.s.) sample was defined as follows:

$$\begin{aligned} &\mathrm{CC}{>}0.0, \quad B_s^{**0} \to B^+K^-, \ \text{'right-sign'} \\ &\mathrm{CC}{<}0.0, \quad B_s^{**0} \to B^+K^+, \ \text{'wrong-sign'}. \end{aligned}$$

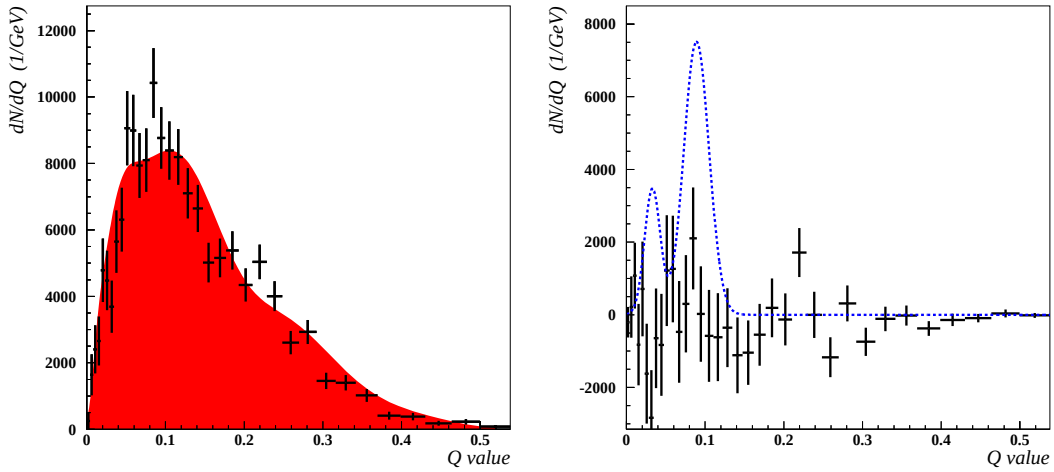

Figure 13: The left-hand plot shows a $\Sigma_b^{(*)}$ enhanced Q-value distribution and the right-hand plot the background subtracted off, together with a comparison with the old DELPHI result giving a total production rate of 4.8%. The upper limit given in the text corresponds to the region at a Q-value of 80 MeV.

Extracting the B_s^{**} rate

The B_s^{**} production rate, $f(B_s^{**})$, was determined by subtracting the r.s. distribution in a Monte Carlo sample for which the B_s^{**} content was removed, from that measured in the data. The production rate in the w.s. sample, which is expected to be consistent with zero, was also measured as a crosscheck in the same way as for the right-sign sample.

The resulting distribution was corrected by the acceptance and filled into a histogram with variable binning, with the bin size adjusted to half of the resolution at a given Q-value. The production rate was determined in a scan over the range of 0.0 to 150.0 MeV in Q-value by fitting single Gaussians to the distribution at equidistant steps with the mean and width constrained to the parameters expected at the specific Q-value.

The fit giving the largest rate in the scan is used for the calculation of the upper limit. The result for the B_s^{**} -rate is given by

$$f(B_s^{**}) < 1.02\% \quad @ \quad 95\% \text{ CL}$$

at a Q-value of 70 MeV (figure 12). For narrow resonances at other Q-values in the interval from 0 to 150 MeV, the limit is even smaller. Further systematic investigations are under way.

Selection of $\Sigma_b^{(*)}$ Events

In the search for $\Sigma_b^{(*)}$ events a 'right-sign' and 'wrong-sign' sample definition was not performed, since no separation can be made for the $\Sigma_b^{(*)+}$ and $\Sigma_b^{(*)-}$ states. The

enhancement was performed by a dedicated $\Sigma_b^{(*)}$ neural network trained to separate pions, coming from the $\Sigma_b^{(*)}$ decay, from every other track. The weak decaying state had to be compatible with a Λ_b baryon. Λ_b were identified by the Λ_b output node of the BHBN network described in [24].

Extracting the $\Sigma_b^{(*)}$ rate

The $\Sigma_b^{(*)}$ production rate, $f(\Sigma_b^{(*)})$, was determined in the same way as for the B_s^{**}, giving an upper limit result of

$$f(\Sigma_b^{(*)}) < 0.97\% \quad @ \quad 95\% \text{ CL.}$$

at a Q-value of 80 MeV (figure 13).For narrow resonances at other Q-values in the interval from 0 to 150 MeV, the limit is even smaller. Further systematic investigations are necessary.

5 Summary and Conclusion

New analyses on excited b states using larger statistics, a completely revised track reconstruction and improved techniques increasing the purity and reducing the dependence on the background modelling have been presented. The production rate of a component compatible with the detector resolution - which suggests the interpretation that it stems mainly from narrow $B_{u,d}^{**}$ states only - has been measured within the High Efficiency Approach to

$$\frac{\sigma(B_{u,d}^{**})_{narrow}}{\sigma_b} = 0.098 \pm 0.007 \pm 0.012$$

The data suggests the presence of broad states with an indication of spin-orbit-inversion.

For B_s^{**} and $\Sigma_b^{(*)}$ upper limits on the production rates have been obtained:

$$\sigma(B_s^{**})/\sigma_b < 0.015, \quad \sigma(\Sigma_b^{(*)})/\sigma_b < 0.015 \quad @ \quad 95\% \text{ CL}$$

These limits supersede previous DELPHI results. Note that all results are preliminary.

Further investigations are going on especially concerning the exact composition of the high mass excess in data of the High Purity Approach and possible small signals of B_s^{**} and $\Sigma_b^{(*)}$.

References

[1] DELPHI Collab., P. Abreu et al., Phys. Lett. **B345** (1995) 598.

[2] DELPHI Collaboration, M. Feindt, C. Kreuter and O. Podobrin, Observation of orbitally excited B and B_s mesons, Contribution to the EPS HEP 1995 conference Brussels, ref eps0563, DELPHI 95-105, PHYS 540.

[3] N. Isgur, M.B. Wise, Phys. Lett. **B232** (1989) 113; Phys. Lett. **B237** (1990) 527; 'Heavy Quark Symmetry' in *B Decays*, 2nd edition, ed. S. Stone (World Scientific, 1994), 231.

[4] M. Gronau, A. Nippe and J. Rosner, Phys. Rev. **D 47** (1993) 1988.

[5] CDF Collab., F. Abe et al., Phys. Rev. Lett. **80** (1998) 2057; CDF Collab., F. Abe et al., Phys. Rev. **D 59** (1998) 032001; CDF Collab., F. Abe et al., Phys. Rev. Lett. **81** (1998) 5513; CDF Collab., T. Affolder et al., Phys. Rev. **D 61** (2000) 072005;

[6] ALEPH Collab., R. Barate et al., Phys. Lett. **B 425** (1998) 215.

[7] DELPHI Collab., P. Abreu et al., Z. Phys. **C 68** (1995) 353. OPAL Collab., K. Akerstaff et al., Z. Phys. **C 74** (1997) 413.

[8] ALEPH Collab., D. Buskulic et al., Z. Phys. **C 69** (1996) 393;

[9] CDF Collab., T. Affolder et al., Phys. Rev. **D 64** (2001) 072002.

[10] J. L. Rosner Comm. Nucl. Part. Phys. **16** (1986) 109; N. Isgur and M.B. Wise, Phys. Rev. Lett. **66** (1991) 1130.

[11] OPAL Collab., R. Akers et al., Z. Phys. **C 66** (1995) 19.

[12] E.J. Eichten, C.T. Hill and C. Quigg, Phys. Rev. Lett. **71** (1993) 4116,
E.J. Eichten, C.T. Hill and C. Quigg, Fermilab Conf 94/118 T.

[13] L3 Collab., M. Acciarri et al., Phys. Lett. **B465** (1999) 323.

[14] ARGUS Collab., H Albrecht et al., Phys. Rev. Lett. **56** (1986) 549; ARGUS Collab., H Albrecht et al., Phys. Lett. **B 221** (1989) 422; ARGUS Collab., H Albrecht et al., Phys. Lett. **B 231** (1989) 208; ARGUS Collab., H Albrecht et al., Z. Phys. **C 69** (1996) 405; CLEO Collab., P. Avery et al., Phys. Rev. **D 41** (1990) 774; CLEO Collab., J. Alexander et al., Phys. Lett. **B 303** (1993) 377; CLEO Collab., P. Avery et al., Phys. Lett. **B 331** (1994) 236; CLEO Collab., T. Bergfeld et al., Phys. Lett. **B 340** (1994) 194; CLEO Collab., Y. Kubota et al., Phys. Rev. Lett. **72** (1994) 1972; E691 Collab., P. E. Karchin et al., Phys. Rev. Lett. **62** (1989) 1717; E687 Collab., P. L. Frabetti et al., Phys. Rev. Lett. **72** (1994) 324; BEBC Collab., W. Burkot et al., Z. Phys. **C 61** (1994) 563; OPAL Collab., R. Akers et al., Z. Phys. **C 67** (1995) 57; OPAL Collab., K. Akerstaff et al., Z. Phys. **C 76** (1997) 425; ALEPH Collab., D. Buskulic et al., Phys. Lett. **B 345** (1994) 103; ALEPH Collab., D. Buskulic et al., Z. Phys. **C 62** (1994) 1; ALEPH Collab., D. Buskulic et al., Z. Phys. **C 73** (1997) 601.

[15] S. Godfrey and R. Kokoski, Phys. Rev. **D** (1991) 1679.

[16] M. Gronau and J. L. Rosner, Phys. Rev. **D 49** (1994) 254.

[17] S.N. Gupta and J.M. Johnson, Phys. Rev. **D 51** (1995) 168.

[18] A. F. Falk and T. Mehen, Phys. Rev. **D 53** (1996) 231.

[19] N. Isgur, Phys. Rev. **D 57** (1998) 4041.

[20] D. Ebert, V.O. Galkin and R. N. Faustov, Phys. Rev. **D 57** (1998) 5663.

[21] DELPHI Collab., P. Abreu et al., Z. Phys. **C 68** (1995) 541,
ALEPH Collab., D. Buskulic et al., Phys. Lett. **B 384** (1996) 449.

[22] DELPHI Collaboration, Nucl. Instr. and Meth. **A303**(1991) 233;

[23] DELPHI Collaboration, Nucl. Instr. and Meth. **A378**(1996) 57.

[24] Z. Albrecht, T. Allmendinger, G. Barker, M. Feindt, C. Haag, M. Moch, *BSAURUS-A Package For Inclusive B-Reconstruction in DELPHI* , hep-ex/0102001.

[25] DELPHI Collaboration, A study of B_s - $\overline{B_s^0}$ oscillations, contribution to ICHEP 2002 Amsterdam, paper 587, DELPHI note 2002 073 CONF 607.

[26] Z. Albrecht, M. Feindt, M. Moch, *MACRIB, high efficiency, high purity hadron identification for DELPHI*, hep-ex/0111081.

[27] DELPHI Collaboration, P. Aarnio et al., Nucl. Inst. Meth. **A303**(1991) 233,
DELPHI Collaboration, P. Abreu et al., Nucl. Inst. Meth. **A378**(1996) 57.